remote sensing

MDPI

Article

ANFIS-EKF-Based Single-Beacon Localization Algorithm for AUV

Wanlong Zhao [1], Huifeng Zhao [2], Gongliang Liu [1,*] and Guoyao Zhang [1]

[1] School of Information Science and Engineering, Harbin Institute of Technology, Weihai 264200, China
[2] College of Underwater Acoustic Engineering, Harbin Engineering University, Harbin 150009, China
* Correspondence: liugl@hit.edu.cn

Abstract: Singe-beacon localization technology can help Autonomous Underwater Vehicles (AUVs) to obtain precise positions by deploying only one beacon. It is considered as a promising way, benefiting from saving much time and labor compared with traditional Long-Baseline Localization (LBL). A typical single-beacon localization scheme contains two essential questions: the initial observability problem and long-endurance trajectory tracking problem. Aiming at these core problems, a comprehensive solution for single-beacon localization is described in this paper. An multi-hypothesis initial position discriminant method is proposed firstly, which helps to achieve accurate initial location based on observability analysis. Then, an Adaptive Network Fuzzy Inference System (ANFIS)-improved Extended Kalman Filter (EKF) method is proposed, in which single-beacon measuring information is fused with off-the-shelf sensors, including DVL, Compass, etc. ANFIS-EKF can help to improve trajectory tracking precisions by restraining the heavy loss of linearization in conventional EKF. Both simulation and field tests are conducted to verify the performance of the proposed algorithms.

Keywords: single-beacon localization; EKF; ANFIS; AUV; observability analysis

check for updates

Citation: Zhao, W.; Zhao, H.; Liu, G.; Zhang, G. ANFIS-EKF-Based Single-Beacon Localization Algorithm for AUV. *Remote Sens.* **2022**, *14*, 5281. https://doi.org/10.3390/rs14205281

Academic Editors: Fabio Menna and Andrzej Stateczny

Received: 24 August 2022
Accepted: 20 October 2022
Published: 21 October 2022

1. Introduction

In recent years, AUV has been widely used in underwater operations benefiting from that it can execute underwater diversified tasks more conveniently to meet the needs of underwater technology advances. During underwater missions, precise location information of AUV is one of the most essential elements of ocean operations, including data observation, target tracking, etc. Due to the rapid decay of wireless signals in underwater environments, Global Navigation Satellite Systems (GNSSs) are disabled, especially in deep sea areas [1]. Hence, various underwater acoustic positioning technologies have been investigated for underwater localization. There are two common underwater acoustic positioning systems, including Long Baseline (LBL) and Ultra-short Baseline (USBL) positioning systems in actual operations. The operating range of USBL is always much closer than LBL; therefore, the LBL system is usually utilized for prolonged and long-distance missions. However, four beacons at least should be deployed and calibrated in advance in conventional LBL positioning systems. Considering saving the consumption of time and labor, an underwater single-beacon localization method is developed for AUV localization.

Single-beacon localization has attracted more and more attention recently on account of that it utilizes only one beacon's ranging information to calculate the location of AUVs, with the help of velocity information from Doppler Velocity Log (DVL), heading information from compasses, etc. A single-beacon localization scheme was proposed firstly by A. P. Scherbatyuk in 1995 [2]. Then, multiple localization methods assisted by single beacons have been studied further, and their application scenarios are also more extensive. Filtering estimation methods are the most common solutions for single-beacon localization, which adopts previous state information to estimate current state information. J. Vaganay et al. designed a Least Square (LS) and EKF method to obtain initial location and to predict underwater vehicle position [3]. The literature in [4] proposes a sum of Gaussian single-beacon range-only localization schemes, which combine EKF and Particle Filter (PF) to estimate unknown state. A KF-based double-integrator system is designed with augmented state in [5]. The literature in [6] adopts a novel KF method to estimate location by adding sound velocity into a state variable. For single-beacon tracking divergence problems, an adaptive KF-based single-beacon tracking algorithm is proposed in [7]. A water velocity bias estimator based on EKF and PF is proposed to enhance localization accuracy further in [8]. An expectation maximization method is used to estimate the unknown effective sound velocity by treating it as a model parameter in [9], which adopts KF for position estimation. A new EKF method including Inertial Measurement Unit (IMU) bias estimation is applied in [10]. The literature in [11] fuses the Rauch–Tung–Striebel smoother into EKF, and a linear time-varying single-beacon navigation model is used to enhance KF performance in [12]. In addition to filtering estimation methods, there are many other methods that can be used for single-beacon localization, such as modified LS [13,14], Cayley–Menger determinant configuration [15], the second-order time difference of arrival model [16], the phase difference coordinate solution equation [17], and virtual LBL [18–20]. In addition, PF can also be used solely to track an underwater target from a maneuver surface vehicle, but the computation complexity is much greater than EKF [21]. Although the filtering estimation method has been proved to work well in single-beacon localization from previous studies, the majority of studies only focus on improvement of localization performance ignoring the initial observability and initial location problems. Additionally, fast-growing deep learning methods have been proved to play a significant role in optimizing algorithms, which is considered a promising way to solve underwater localization problems. The literature in [22] proposes a novel underwater localization method by combining Radial Basis Function (RBF) and Error-state Kalman Filter (ESKF). A Recurrent Neural Network (RNN) and EKF joint algorithm is proposed in [23]. In both of these two methods, an intelligent network is adopted to correct filtering errors. Moreover, a supervised-learning-based adaptive tuning scheme to select the proper INS step size is designed in [24]. However, to the best of the authors' knowledge, there are few deep learning methods applied in single-beacon localization technology suitably till now. ANFIS combines the adaptive network and fuzzy inference system organically, which has been applied in various fields [25]. Benefiting from fast convergence rate, strong fitting and prediction ability, and stable mapping relationships [26,27], in our view, ANFIS owns significant potential in single-beacon localization technology. Hence, this paper aims to design a complete improved algorithm by combing filtering estimator and ANFIS for single-beacon localization, which considers both the initial observability problem and long-endurance trajectory tracking problem adequately.

The contributions of this paper are shown as follows. A comprehensive solution is designed for AUV localization with the aid of a single beacon. Firstly, the observability analysis of single-beacon localization is conducted, which lays a foundation for whether a certain single-beacon localization method can be used in a nonlinear positioning process. Then, a Multi-hypothesis Initial Position Discriminant (MHIPD) method is put forward to estimate the initial position of the AUV, which helps to overcome the inherent shortage that only one series of acoustic ranging information can be used from a single beacon. Eventually, an improved Extended Kalman Filter (EKF) algorithm based on an Adaptive Network Fuzzy Inference System (ANFIS) is proposed for underwater single-beacon localization. The proposed ANFIS-EKF scheme can help to maintain high-precision trajectory tracking in long-endurance operations of AUVs.

The rest of this paper is organized as follows. Section 2 introduces the framework of a single-beacon localization system, presents the observability analysis method, and describes proposed initial position discriminant and trajectory tracking algorithms minutely. In Section 3, the performances of the proposed MHIPD and ANFIS-EKF methods are analyzed by simulations and experiments successively. Finally, conclusions are given in Section 4.

2. Methods

2.1. Framework of Single-Beacon Localization System

A single-beacon localization system depends on transmission delay measuring of an acoustic signal to estimate ranging information between AUV and a single beacon. In single-beacon-based AUV localization, the AUV updates its position estimation by fusing velocity information and ranging information. Figure 1 shows a framework of a typical single-beacon localization system, in which a single beacon is deployed at the bottom of the sea. From Figure 1, it is clear that on one hand, this single-beacon localization system is much simpler compared with LBL, which contributes an obvious advantage of less deployment cost; on the other hand, the seafloor single beacon can help AUVs to avoid rising to the sea surface for position calibration in long-endurance operations in deep sea. Hence, seafloor single beacons can improve the concealment of AUVs compared with an autonomous surface vehicle or buoy.

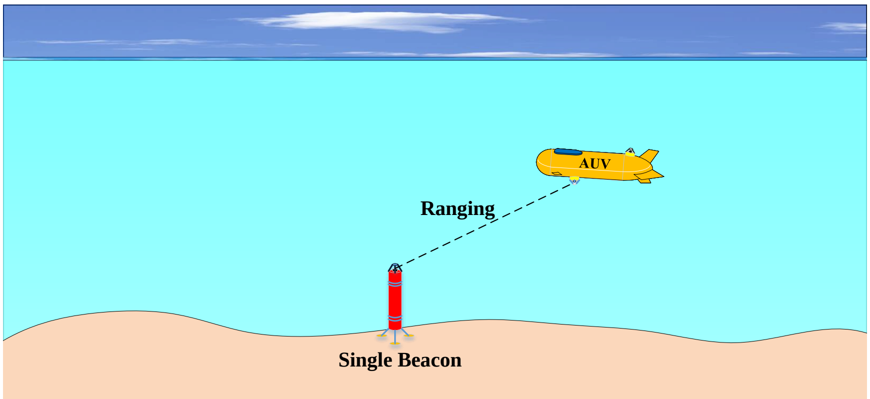

Figure 1. Illustration of framework of single-beacon localization.

In the framework of single-beacon localization, AUVs always move in deep sea environments when performing long-distance operations. To realize AUV state estimation, various off-the-shelf sensors are employed, including DVL, compasses, pressure sensors, etc., which can provide velocity, heading, and depth information, respectively. Due to depth information generally being able to be accurately measured by pressure sensor, a two-dimension environment is considered in the following section of this paper. In this paper, there are no explicit requirements for performance of DVL and compasses. Admittedly, when the precision of DVL and compasses are better, the localization performance is better. During the experiment, DVL and compasses are considered to satisfy the localization operation precision, which can be used directly without preprocessing. Additionally, sound velocity is considered as a constant in this paper for convenience.

2.2. Observability Analysis

The purpose of observability analysis is to verify whether and when the single-beacon localization method can be used suitably for AUV. Generally, a system is considered to be observable when the state of the system can be uniquely determined in finite time from its inputs. In other words, observability is used to verify whether information from measured variables is sufficient to estimate the state. Due to underwater localization systems being mostly nonlinear, a Lie derivative observability analysis method for single-beacon localization is conducted.

A typical nonlinear system can be described as

$$\begin{aligned} x(t) &= f(x(t), u(t)),\ x(t_0) = x_0 \\ y(t) &= h(x(t)) \end{aligned} \tag{1}$$

where $x \in R^N, u \in R^Q, and y \in R^M$ present states, inputs, and outputs, respectively. t indicates time slot. Aiming to analyze observability, an observability matrix is designed based on Lie derivatives, which is defined as shown in Equation (2).

$$\begin{aligned}
&L_f^0(h_j) = h_j \\
&L_f^1(h_j) = \triangledown h_j \cdot f = \sum_{i=1}^{N} \frac{\partial h_j}{\partial x_i} \cdot f_i \\
&\quad\vdots \\
&L_f^l(h_j) = \triangledown[L_f^{l-1}(h_j)] \cdot f
\end{aligned} \tag{2}$$

Hence, we can obtain the observability matrix, shown as Equation (3)

$$\mathbf{O} = \begin{bmatrix} \triangledown L_f^0(h_1) & \cdots & \triangledown L_f^0(h_m) \\ \triangledown L_f^1(h_1) & \cdots & \triangledown L_f^1(h_m) \\ \vdots & \ddots & \vdots \\ \triangledown L_f^{n-1}(h_1) & \cdots & \triangledown L_f^{n-1}(h_m) \end{bmatrix} \tag{3}$$

where $L_f^a(h_j)$ represents the a order Lie derivatives for $j \in 1, \ldots, m$, and $\triangledown$ denotes the gradient operator.

According to the feature of the Lie derivative, a nonlinear system is considered to be locally weakly observable when its observability matrix owns full rank. Based on the above theory, the observability analysis of single-beacon localization is shown as follows.

The state variable of the single-beacon localization system is defined as $\mathbf{x} = [x, y]^{\mathrm{T}}$, where x, y represent the two-dimensional coordinates of the AUV. The system state model is defined as

$$\begin{aligned}
x_k &= x_{k-1} + v_{k-1} \times cos(\phi_{k-1}) \times \Delta t \\
y_k &= y_{k-1} + v_{k-1} \times sin(\phi_{k-1}) \times \Delta t
\end{aligned} \tag{4}$$

where v_{k-1} and ϕ_{k-1} represent velocity and heading at time slot $k-1$, respectively. Δt presents update period. Then, the nonlinear state equation can be presented as

$$\mathbf{x}_k = f(\mathbf{x}_{k-1}, u_{k-1}) + w_k \tag{5}$$

where $f(\mathbf{x}_{k-1}, u_{k-1}) = \begin{bmatrix} x_{k-1} \\ y_{k-1} \end{bmatrix} + \begin{bmatrix} v_{k-1}cos(\phi_{k-1}) \\ v_{k-1}sin(\phi_{k-1}) \end{bmatrix} \Delta t$, and w_k represents system noise. According to system model, the state equation can be further described as

$$\dot{\mathbf{x}} = f(\mathbf{x}, u) \tag{6}$$

where $f = \begin{bmatrix} f_1 \\ f_2 \end{bmatrix} = \begin{bmatrix} v_{k-1}cos(\phi_{k-1}) \\ v_{k-1}sin(\phi_{k-1}) \end{bmatrix}$.

Because the measurement information of the single-beacon localization system is one-time one-point ranging information, namely $m = 1$, m presents the number of measurements. Hence, the measurement equation can be described as

$$h_1 = \sqrt{(x_b - x_k)^2 + (y_b - y_k)^2} \tag{7}$$

where x_b, y_b are the single-beacon position coordinates. Then, each order Lie derivatives are shown as follows.

$$\begin{aligned}
&L_f^0(h_1) = h_1 \\
&L_f^1(h_1) = \frac{x_b - x_k}{h_1} f_1 + \frac{y_b - y_k}{h_1} f_2
\end{aligned} \tag{8}$$

The gradients of each order Lie derivatives are calculated as

$$\begin{aligned}\bigtriangledown L_f^0(h_1) &= \begin{bmatrix} \frac{x_b-x_k}{h_1} & \frac{y_b-y_k}{h_1} \end{bmatrix} \\ \bigtriangledown L_f^1(h_1) &= \begin{bmatrix} \frac{(y_b-y_k)^2 f_1-(x_b-x_k)(y_b-y_k)f_2}{h_1^3} \\ \frac{(x_b-x_k)^2 f_2-(x_b-x_k)(y_b-y_k)f_1}{h_1^3} \end{bmatrix}^{\mathrm{T}}\end{aligned} \tag{9}$$

Put Equation (9) into Equation (3), then the observability matrix $\mathbf{O}$ can be achieved. If the single-beacon localization system is observable, its observability matrix should satisfy

$$det(\mathbf{O}) = \frac{f_2(x_b - x_k) - f_1(y_b - y_k)}{h_1^2} \neq 0 \tag{10}$$

From Equation (10), it can be seen that when the AUV moves in a straight line towards the single beacon or keeps still all the time, $det(\mathbf{O})$ will equal 0, then the system will be unobservable.

In order to further analyze system observability, the observability degree based on spectral condition number is utilized in this paper, which can calculate and compare system observability quantitatively. Firstly, the observability matrix is decomposed by singular value decomposition theorem, shown as

$$\mathbf{O} = \mathbf{USV}^{-1} \tag{11}$$

where $\mathbf{U}, \mathbf{V}$ are the orthogonal matrix, and $\mathbf{S} = diag(\sigma_1, \sigma_2, \cdots, \sigma_r)$ is the singular value diagonal matrix of observability matrix. According to spectral condition number theory, let the spectral condition number $\kappa_2(\mathbf{O})$ of the observability matrix present the observability degree of single-beacon localization, shown as

$$\kappa_2(\mathbf{O}) = \frac{max_{\sigma\in\sigma(\mathbf{O})}|\sigma|}{min_{\sigma\in\sigma(\mathbf{O})}|\sigma|} \tag{12}$$

In order to let the observability degree be a positive integer less than or equal to 1 for the convenience of mathematical statistics, the observability degree is further defined as the inverse of the spectral condition number of the observability matrix.

$$\frac{1}{\kappa_2(\mathbf{O})} = \sqrt{\frac{\min(|v_{k-1}((y_b - y_k)\cos\phi_{k-1} - (x_b - x_k)\sin\phi_{k-1})/h_1^2|, 1)}{\max(|v_{k-1}((y_b - y_k)\cos\phi_{k-1} - (x_b - x_k)\sin\phi_{k-1})/h_1^2|, 1)}} \tag{13}$$

Based on Equation (13), the observability degree can be obtained on account of multi-parameters, including position, velocity, heading, etc. Let α be the angle between x coordinate axis and the connecting line between the current position of the AUV and the position of the single beacon, then $\alpha - \phi$ is defined as deviation angle, which indicates the degree of deviation between heading direction and relative positioning of the AUV's single beacon. The observability degree can be finally expressed as

$$\frac{1}{\kappa_2(\mathbf{O})} = \sqrt{\frac{\min(v_{k-1}\sin(\alpha - \phi_{k-1})/h_1, 1)}{\max(v_{k-1}\sin(\alpha - \phi_{k-1})/h_1, 1)}} \tag{14}$$

From the above analysis, it is seen that the bigger the observability degree is, the better the initial observability is. Actually, the observability degree of the single-beacon localization system is affected by different kinds of measurements, including velocity measuring, heading measuring, transmission delay, etc. This causes transmission delay, making an impact on ranging information; hence, velocity, heading angle, and ranging are selected to estimate the observability degree in this method. Furthermore, a simulation is conducted to analyze the relationships between velocity, deviation angle, ranging, and observability degree, as shown in Figure 2.

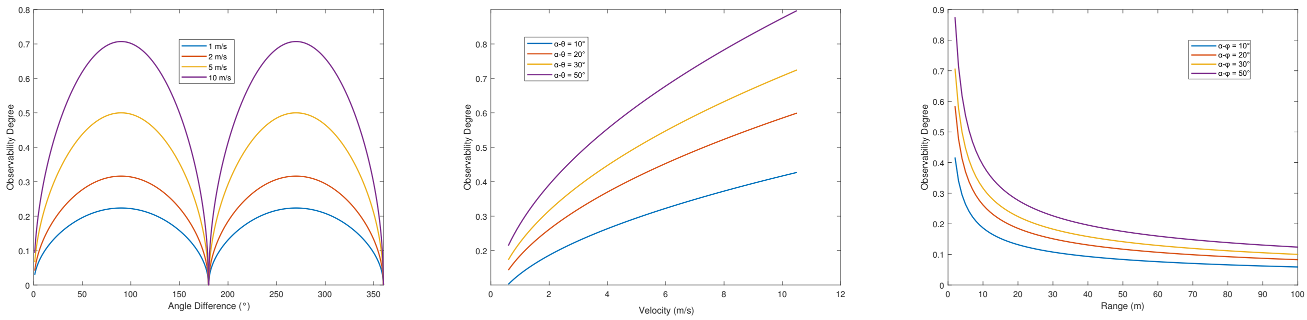

(**a**) (**b**) (**c**)

Figure 2. The relationships between different parameters and observability degree. (**a**) Relationship between heading angle and observability degree. (**b**) Relationship between velocity and observability degree. (**c**) Relationship between ranging and observability degree.

Figure 2a gives the relationship between deviation angle and observability, from which it can be seen that observability degree is 0 when heading angle equals to $0°$,$180°$, and $360°$. The same results appear from the former analysis of Equation (10). Figure 2b gives the relationship between velocity and observability; it is clear that observability degree increases with increasing velocity information. From Figure 2c, it is concluded that the smaller the ranging is, the bigger the observability degree is.

2.3. MHIPD

Based on the above analysis, it is known that the observability of single-beacon localization is varying, as measured by the observability degree. During the whole positioning process, the most important node of observability is initial observability, which is decided by how to achieve accurate initial position.

As mentioned before, the scenario of long-endurance trajectory tracking in deep seas is considered; hence, AUVs cannot emerge from the water to obtain GPS calibration. As a result, initial location should be estimated by the information from its own sensors and range information with the single beacon, which owns the accurate location. It is known that the initial location cannot be measured accurately at the first time-slot of acoustic transmission delay from a single beacon. One thing is certain, AUVs locate on the surface of a ball whose center is a single beacon and whose radius ranges from the single beacon. Considering two-dimensional coordinates, the initial position locates on a circle, the center of which is the projection point of the single beacon. In order to ensure exact initial position further, a series of transmission delays in the next several time-slots always needs to be used. The purpose of using several time-slots for the initial estimation is to employ time-consuming exchanges for initial position precision. However, even at the expense of many time-slots, initial observability is poor on account of the measuring error and misleading mirror solutions.

Aiming at the initial observability problem, a Multi-hypothesis Initial Position Discriminant (MHIPD) method is designed. In the MHIPD method, a new variable Positioning Angle Accuracy (PAA) is designed as θ. According to multi-hypothesis theory, each θ degree is considered as a hypothetical initial position, which means that there will be $i = 360^o/\theta$ potential initial positions. An illustration of PAA is shown in Figure 3.

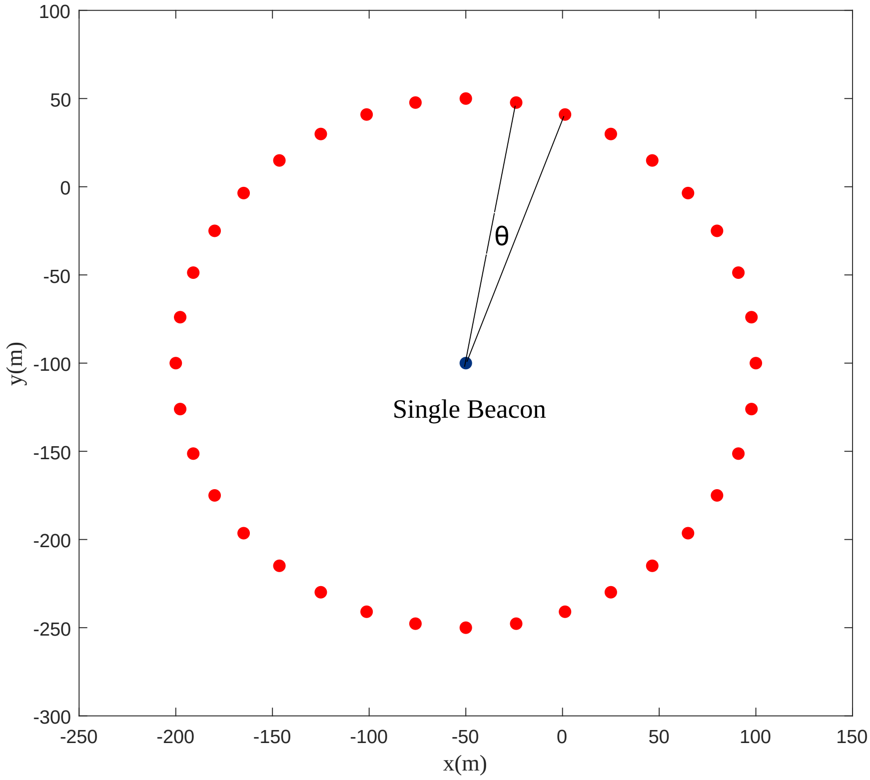

Figure 3. Illustration of PAA in MHIPD method.

Based on the PAA supposing method, the initial observability problem is transformed to find the most likely one among potential initial positions.

For each potential initial position, the next time position can be obtained based on velocity information as follows.

$$\begin{aligned} x_1^i &= x_0^i + v_{x,0} \times \Delta t \\ y_1^i &= y_0^i + v_{y,0} \times \Delta t \end{aligned} \tag{15}$$

where x_0^i, y_o^i denote the coordinates of the i_{th} hypothetical position at initial time, x_1^i, y_1^i present coordinates of the i_{th} hypothetical position at adjacent followed time, and $v_{x,0}, v_{y,0}$ present motion velocity in x and y direction at initial time, respectively. Then, a calculated ranging can be obtained from each next time position and single-beacon position.

$$d_1^i = \sqrt{\left(x_1^i - x_b\right)^2 + \left(y_1^i - y_b\right)^2 + \left(z_1 - z_b\right)^2} \tag{16}$$

where d_1^i represents ranging information of the i th hypothetical position at adjacent followed time, x_b, y_b, z_b present single-beacon position coordinates, and z_1 is the depth information measured by pressure sensor. Meanwhile, a measurement ranging between the AUV and the single beacon can be achieved by transmission delay from the single beacon at adjacent followed time; hence, an error e_1^i between two rangings can be calculated, which can assist us to figure out the real initial position.

$$e_1^i = \mid d_1^i - c \times \tau_1 \mid \tag{17}$$

where e_1^i denotes the error of the i th hypothetical position, τ_1 is transmission delay at adjacent following time, and c represents sound velocity, respectively.

According to the above method, more errors $e_k^i, k = 1, 2, 3...$ can be achieved between rangings in the next and next adjacent following time, in which k stands for calculating times in the initial position calculating process.

Generally speaking, the initial position of minimum error should most likely be the initial position. However, false judgment still remains caused by measuring noise and misleading mirror solutions. A heuristic principle is designed to overcome the false judgment, in which a count parameter ρ and a threshold value σ are educed, shown as Equation (18).

$$\begin{aligned} &if && e_k^i < \sigma, \\ &then && \rho_i = \rho_i + 1 \end{aligned} \tag{18}$$

where ρ_i is the ith hypothetical position count parameter.

During the initial position calculating process, the count parameter ρ of the position closed to the real initial position will accumulate; the one staying away from the true value tends to conversely be invariable. As the time-slots in the initial position calculating process accumulate, the real initial position will appear, making obvious who owns the maximum count parameter ρ_i. However, because the error is caused by many factors, the result of the count parameter cannot converge to one position in most conditions; the strategy of calculating the mean value of all positions which own a maximum count parameter is applied. Because the position errors are symmetrically distributed on both sides of the truth value, the result has the minimum error.

In the MHIPD method, the selection of calculating times k and threshold σ will affect initial position accuracy greatly, which is discussed further in Section 3.1. What is more, the initial observability is related to the AUV motion trajectory, and there is a popular belief that curve shape has better observability for the estimated target trajectory [28].

2.4. ANFIS-EKF

After obtaining good enough initial observability, another problem of long-endurance trajectory tracking should be considered in single-beacon localization for AUVs. A typical filtering algorithm (EKF) has been widely used in trajectory tracking problems. However, EKF may lose certain positioning accuracy in such a nonlinear localization system due to only the first order nonlinear function being considered. In order to improve the tracking accuracy, an improved EKF based on ANFIS is proposed in this section. Figure 4 gives the flowchart of the proposed ANFIS-EKF.

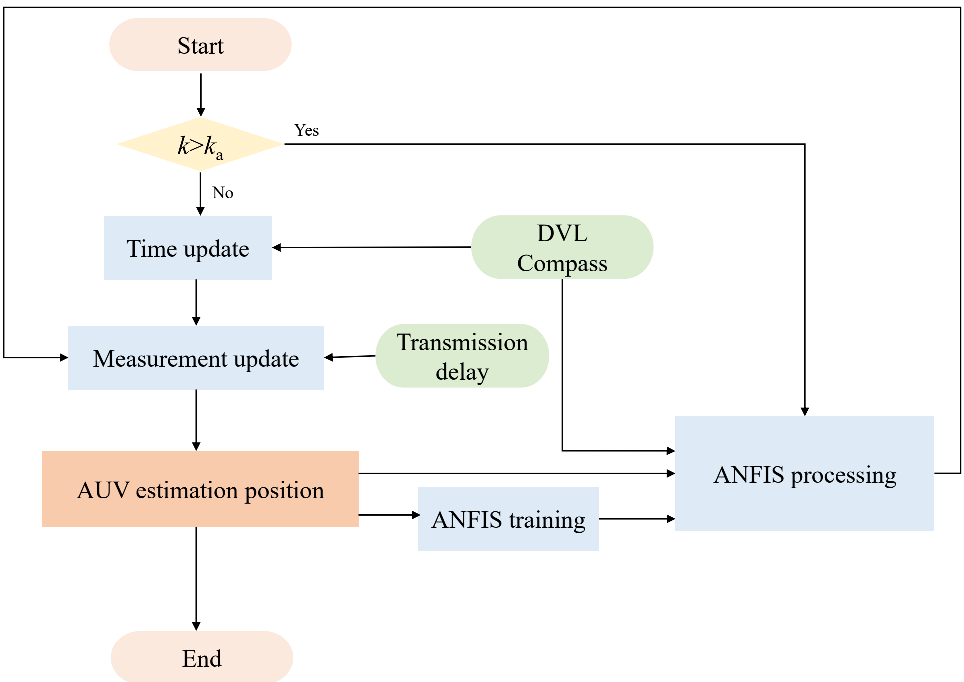

Figure 4. Flowchart of the proposed ANFIS-EKF algorithm.

Due to the building of an accurate model of ANFIS needing more training data, hence before a certain time node k_a, ANFIS only carries on training, rather than participating in the trajectory tracking process. After accomplishing training of the ANFIS model, information measured by DVL and compasses is involved in the ANFIS process, which helps to improve measurement updates of EKF.

There are two phases in EKF, including time update and measurement update. In the time update phase, velocity information is used to predict the system state on the basis of kinematics formula. The time update process is shown as follows:

$$\mathbf{x}_{k|k-1} = f(\mathbf{x}_{k-1}) + w_{k-1} \tag{19}$$

$$\mathbf{P}_{k|k-1} = \mathbf{F}\mathbf{P}_{k-1}\mathbf{F}^{\mathrm{T}} + \mathbf{Q} \tag{20}$$

where $\mathbf{x}_k$ is the dynamic state at time k, f is the same with f in Equation (5), $\mathbf{F}$ is the Jacobian matrix of system update function, $\mathbf{P}_k$ denotes error covariance at time k, w is process noise which is subjected to Gaussian distribution, and $\mathbf{Q}$ is the process noise covariance.

In the measurement update phase, the state and covariance are updated by new a measurement, which represents transmission delay between the single beacon and the AUV.

$$\mathbf{K}_k = \mathbf{P}_{k|k-1}\mathbf{H}^{\mathrm{T}}(\mathbf{H}\mathbf{P}_{k|k-1}\mathbf{P}_{k|k-1} + \mathbf{R})^{-1} \tag{21}$$

$$\mathbf{x}_k = \mathbf{x}_{k|k-1} + \mathbf{K}_k(\mathbf{z}_k - h(\mathbf{x}_{k|k-1})) \tag{22}$$

$$\mathbf{P}_k = (\mathbf{I} - \mathbf{K}_k\mathbf{H})\mathbf{P}_{k|k-1} \tag{23}$$

where $\mathbf{K}$ is the Kalman gain, $\mathbf{H}$ is the Jacobin matrix of the measurement update function, $\mathbf{R}$ is the measurement noise covariance, and $\mathbf{z}$ is the measurement vector.

Single-beacon localization can be considered as a discrete time system. We define a state vector at time k to describe the AUV dynamic state as $\mathbf{x}_k = [x_k, y_k]^{\mathrm{T}}$. Hence, the state update function $\mathbf{F}$ and measurement transition function $\mathbf{H}$ can be described as

$$\mathbf{F} = \begin{bmatrix} 1 & 0 \\ 0 & 1 \end{bmatrix} \tag{24}$$

$$\mathbf{H} = \begin{bmatrix} \frac{x_k - x_b}{v_e\sqrt{(x_k-x_b)^2+(y_k-y_b)^2+(z_k-z_b)^2}} & \frac{y_k - y_b}{v_e\sqrt{(x_k-x_b)^2+(y_k-y_b)^2+(z_k-z_b)^2}} \end{bmatrix} \tag{25}$$

where x_b, y_b, z_b indicate the position coordinates of the single beacon, and v_e is motion velocity of the AUV.

Based on Equation (19)–(25), trajectory tracking can be finished by EKF. However, in conventional EKF, the state prediction function is approximate to the real condition using linear velocity motion in the time update process, which will suffer a loss of localization precision. To improve the accuracy of the state prediction, ANFIS is utilized to train the nonlinear system model.

ANFIS owns two aspects of advantages, one is that the fuzzy inference system can provide outputs by certain rules, and the other is that adaptive networks can learn and adjust network parameters. ANFIS utilizes rules to combine the input, output, and rules. ANFIS is supposed to remodel the relationships between velocity information and state prediction. The diagram of the ANFIS structure is shown in Figure 5.

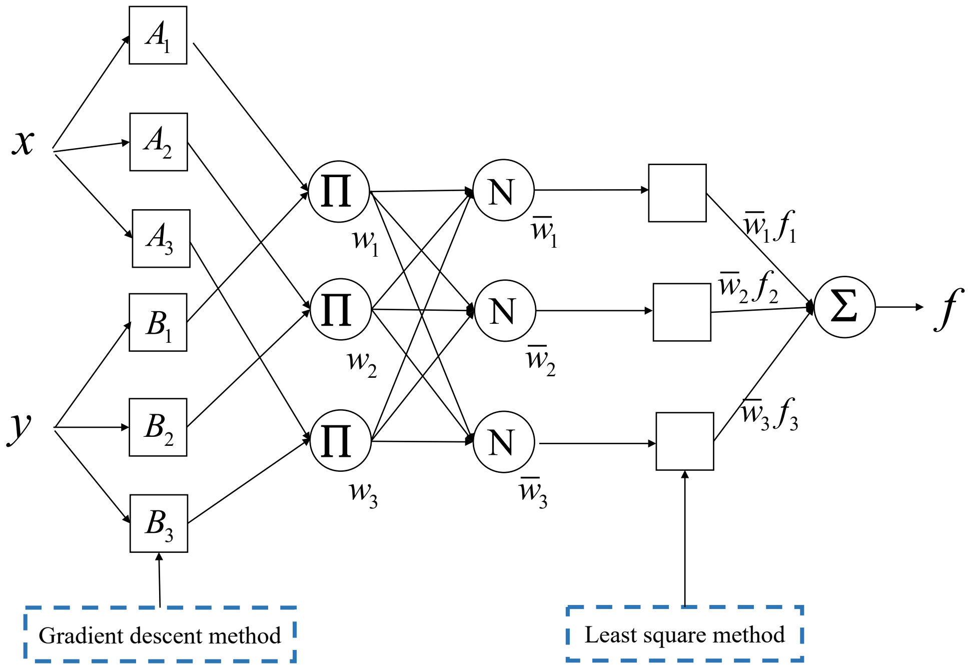

Figure 5. Diagram of the ANFIS structure.

The structure is a five-layer model including fuzzification, rules, normalization, defuzzification, and output layer. Each layer contains a number of nodes with specific functions which are used to determine the relationship between input and output. The circle nodes represent fixed nodes and the square nodes represent adaptive nodes.

A first-order Takagi–Sugeno fuzzy system model is adopted in this paper. In the forward pass of the training process, consequent parameters are updated by the least square method. In the back propagation, the premise parameters are adjusted by the gradient descent method. As a result, ANFIS can be trained to describe nonlinear membership through the iterative adaptive learning process of structure parameters. The five steps of ANFIS are described in detail as follows:

Three rules are adopted in the structure of ANFIS:

$$\begin{aligned} &Rule\,1: \ if\ x = A_1, y = B_1,\ then\ f = p_1x + q_1y + r_1 \\ &Rule\,2: \ if\ x = A_2, y = B_2,\ then\ f = p_2x + q_2y + r_2 \\ &Rule\,3: \ if\ x = A_3, y = B_3,\ then\ f = p_3x + q_3y + r_3 \end{aligned}$$

where A_i, B_i form a fuzzy set and p_i, q_i, and r_i are consequent parameters.

In layer 1, input x and y are fuzzified by membership functions to obtain membership grade. The output of this layer is

$$O_{1,i} = \begin{cases} \mu_{A_i}(x) & i = 1,2,3 \\ \mu_{B_{i-3}}(y) & i = 4,5,6 \end{cases} \tag{26}$$

where μ_{A_i} and $\mu_{B_{i-3}}$ are membership grades.

In layer 2, firing strength is calculated by product of membership grades.

$$O_{2,i} = w_i = \mu_{A_i}(x) \times \mu_{B_i}(y),\ i = 1,2,3 \tag{27}$$

where w_i is the firing strength of the ith rule.

In layer 3, firing percentages of each rule are obtained in rule base.

$$O_{3,i} = \varpi_i = \frac{w_i}{\sum_i w_i},\ i = 1,2,3 \tag{28}$$

In layer 4, fuzzy results of inference input are calculated.

$$O_{4,i} = \varpi_i f_i = \varpi_i (m_i x + p_i y + r_i) \quad (29)$$

Finally, defuzzification results of output are calculated in layer 5.

$$O_{5,i} = \sum \varpi_i f_i = \frac{\sum_i w_i f_i}{\sum_i w_i} \quad (30)$$

Defining measuring error E_p is

$$E_p = \sum_{m=1}^{\#(L)} (T_{m,p} - O^L_{m,p})^2 \quad (31)$$

where $T_{m,p}$ stands for the m_{th} component from p_{th} target output vector, and $O^L_{m,p}$ presents the m_{th} component of L_{th} layer from p_{th} real output vector. Therefore, the total measuring error is $E = \sum_{p=1}^{p} E_p$. Furthermore, the rate of deviation $\partial E_p / \partial O$ between node output O and p_{th} training data is calculated to realize the self-learning process, shown as

$$\frac{\partial E}{\partial O} = -2(T_{i,p} - O^L_{i,p}) \quad (32)$$

If α is a given parameter in an adaptive network, then

$$\frac{\partial E_p}{\partial \alpha} = \sum_{O^* \in S} \frac{\partial E_p}{\partial O^*} \frac{\partial O^*}{\partial \alpha} \quad (33)$$

where S is the a node set whose output depends on α.

Finally, the partial derivation of total measuring error related to α can be achieved after a series of iterations and updates.

Based on the above process, an ANFIS-based transition model can be obtained, which can be considered as a new state transition function used for EKF.

A typical combination of multi-parameters in ANFIS-EKF are given in Table 1.

Table 1. Main parameters of ANFIS structure.

Parameters	Value
Initial fuzzy inference system for training	Grid Partition
Input membership function type	trimf
Output membership function type	linear
Training length	150
Number of Input membership function	3
Error Goal	0.0001

In the next Section, the performance of ANFIS-EKF and the influence of different parameters on ANFIS-EKF are discussed further.

3. Results and Discussion

3.1. Performance Analysis of MHIPD

A single-beacon localization simulation is conducted based on a real lake test scene, shown in Figure 6, where a single beacon is deployed at the bottom of the lake, and a surface ship moves on the lake to pretend to be an AUV. As the surface ship is equipped with GPS, actual initial position can be achieved.

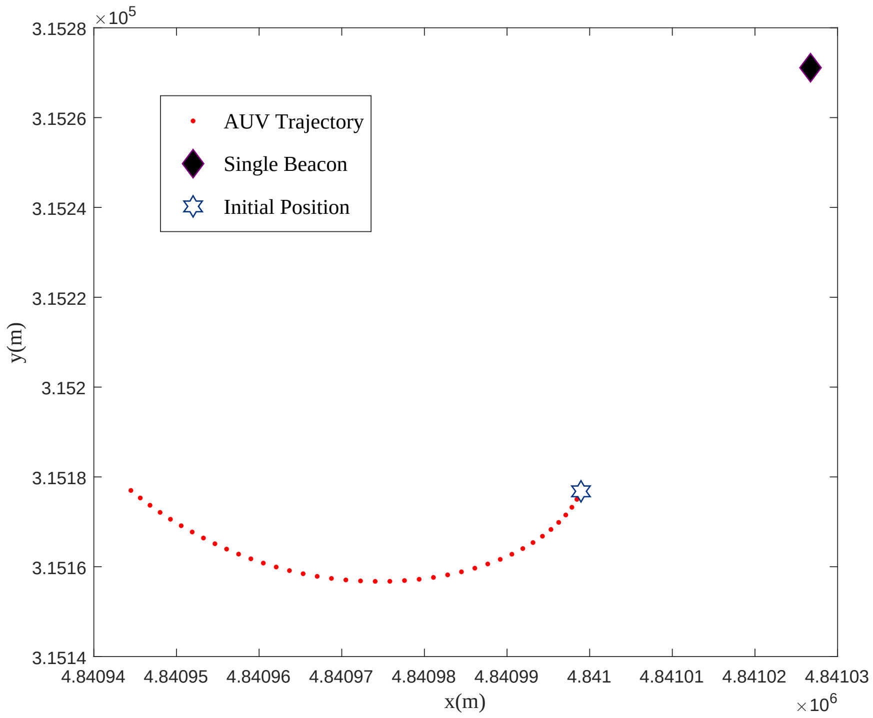

Figure 6. The relationship between the AUV and single beacon.

Simulation parameters are set as follows: transmission delay period between the AUV and single beacon is 4 s, calculating times k is 40, threshold value σ is 4.5 m, and positioning angle accuracy θ is set to be 0.1°.

Figure 7 gives the simulation result, in which count parameter ρ is adopted to find the most suitable angle related to the most accurate initial position. From Figure 7, it can be seen that the count parameter ρ presents a mountain shape, which denotes that the larger the hypothetic position count parameter is, the closer the related potential initial position nears the actual initial position. The maximum ρ appears to be 39 at 253.2°, where the errors of x and y direction between potential initial position and actual initial position are 0.8984m and 0.6500 m, respectively. Such a small initial position error verifies that MHIPD is effective in the initial observability measuring of single-beacon localization.

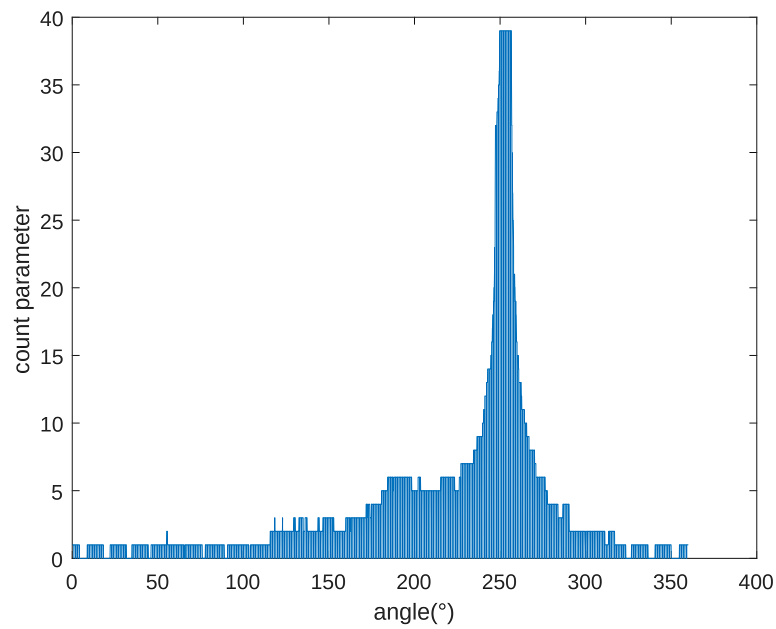

Figure 7. Results of field data of proposed initial position method.

In order to present the performance of MHIPD further, the influence of two parameters are analyzed, including calculating time k and threshold σ .

Firstly, four different calculating times k are tested to see the influence on initial position accuracy, respectively. The simulation results are shown in Figure 8 and Table 2.

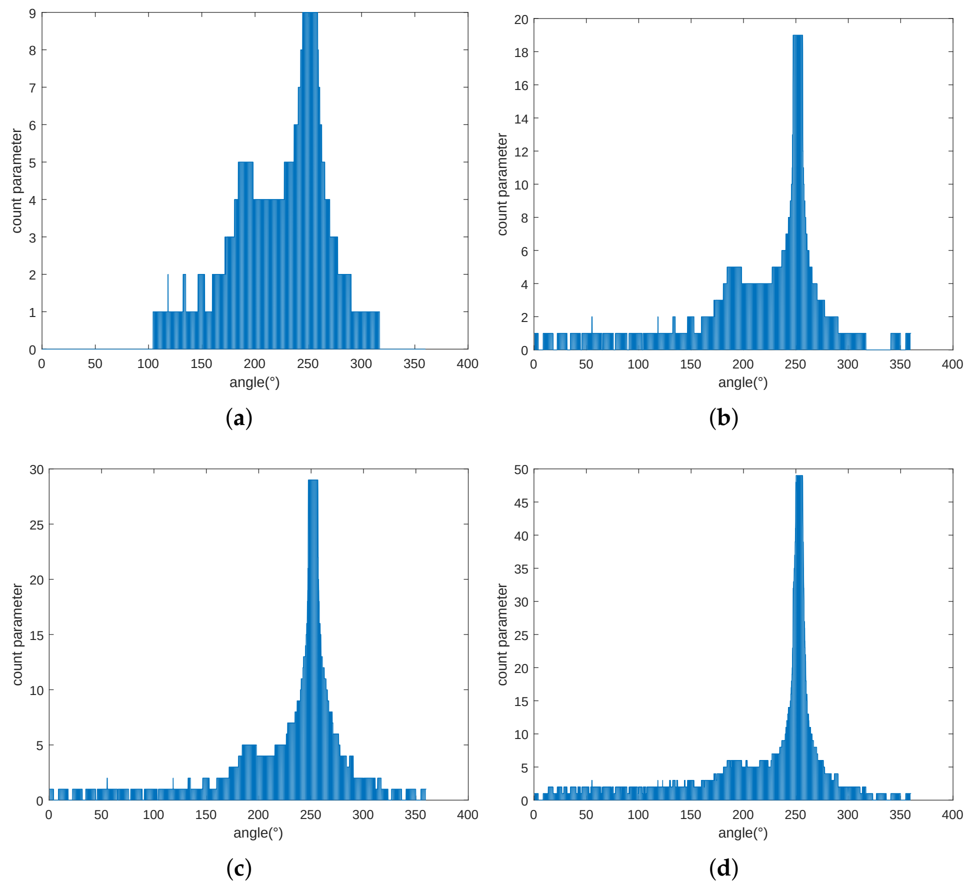

Figure 8. Performance analyzing of different calculation times. (**a**) Calculation times = 10. (**b**) Calculation times = 20. (**c**) Calculation times = 30. (**d**) Calculation times = 50.

Table 2. Simulation results of different calculation times.

Calculating Times k	Error of RMSE (m)	Number of Max Count Parameter	Angle of Initial Position (○)
10	3.5439	128	251.6
20	3.2111	85	251.8
30	3.2111	84	251.8
50	1.1089	60	253.2

From Figure 8, it can be seen that the wave crest becomes narrower as calculation times rise. This causes smaller calculation times, meaning fewer experimental data, which leads to a result that the potential initials near the actual initial owns fewer discriminations from other positions. Therefore, the count parameter ρ is essential to estimate the potential initials in a appropriate period. Table 2 gives more detailed quantitative results. It indicates that the less calculating time is, the bigger the positioning error is, which is caused by the count parameter not reflecting the true relationship between potential initials and the actual initial without enough data. On the other hand, the number of max count parameter decreases as calculating times arises, which is helpful to find the most accurate initial position. Hence, the greater calculating times is, the better performance the MHIPD method owns. However, in real applications, the selection of calculation times should also take computation time into consideration.

Secondly, eight different threshold values σ are tested to see the influence on initial position accuracy, respectively. The simulation results are shown in Figure 9 and Table 3.

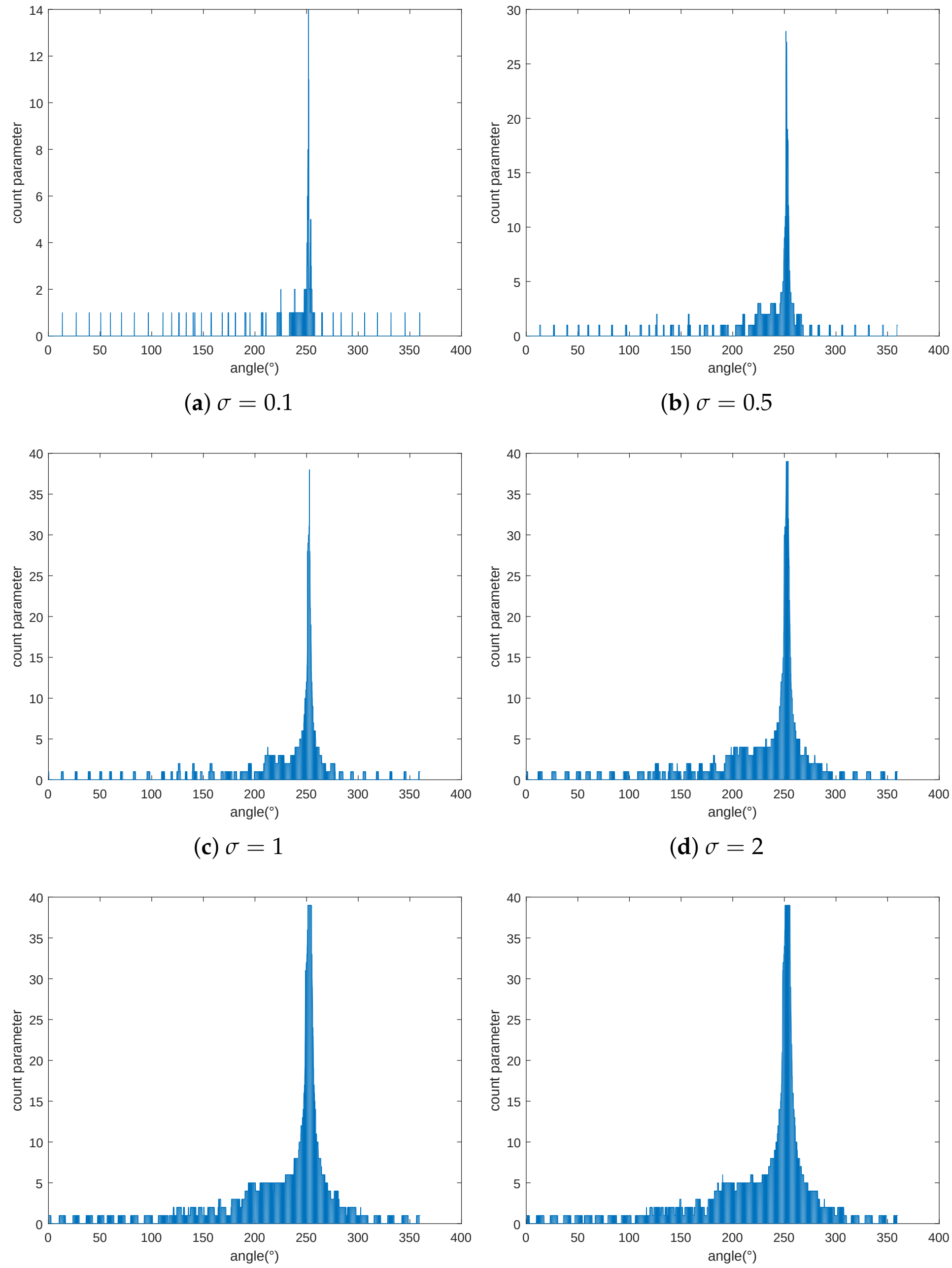

(**a**) $\sigma = 0.1$ (**b**) $\sigma = 0.5$

(**c**) $\sigma = 1$ (**d**) $\sigma = 2$

(**e**) $\sigma = 3$ (**f**) $\sigma = 3.5$

Figure 9. *Cont.*

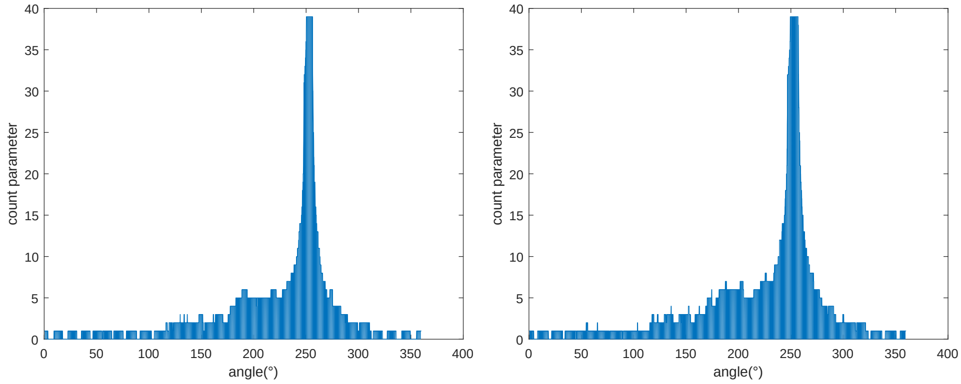

(**g**) $\sigma = 4$ (**h**) $\sigma = 5$

Figure 9. Performance analysis of different threshold values.

Table 3. Simulation results of different threshold values.

Threshold Value σ	Error of RMSE (m)	Number of Max Count Parameter	Angle of Initial Position (○)
0.1	3.0457	1	251.9
0.5	2.5551	6	252.2
1.0	1.7710	2	252.7
2.0	1.4817	19	252.9
3.0	1.3469	36	253.0
3.5	1.2215	45	253.1
4.0	1.2215	53	253.1
5.0	1.1089	69	253.2

From Figure 9, it can be seen that the wave crest widens as thresholds rise. It seems bad because there will be a greater number of max count parameters, namely the existence of more potential initials. However, too small of a threshold value will lead to diminishing initial positioning accuracy, which is confirmed in the 2nd column of Table 3. Hence, the selection of threshold value should take multi-factors into comprehensive consideration. In a real application environment, if calculating times are fixed, threshold value should be as big as possible; under the condition of the number of max count parameters being as small as possible, it is best to be one.

3.2. Performance Analysis of ANFIS-EKF

The performance of ANFIS-EKF is analyzed by field data in this section. A single beacon was deployed in the bottom of "SongHua" Lake, whose position is east longitude 126.91531° and north latitude 43.610448°, and the depth of the single beacon is −209.6 m. In order to calculate positioning error, the latitude and longitude coordinate is transformed into WGS-84 coordinate, hence the position coordinates of the single beacon are (4,841,026.7, 315,271.1, −209.6).

A surface ship is used to replace the AUV to move on the surface of "SongHua" Lake. The ship is equipped with acoustic transmitting and receiving sensors to measure ranging information, DVL to measure velocity, and compasses to measure heading direction. The updating period of the acoustic signal is 4 s. This ship is equipped with Differential GPS (DGPS), which owns centimeter-level high positioning accuracy. Furthermore, DGPS can work in the whole experiment as the ship is moving on the surface of the lake rather than diving into deep water, hence the DGPS results can be considered as the reference trajectory.

To reflect the overall error condition, a distance Root Mean Square Error (RMSE) is adopted to calculate position accuracy. In RMES, the trajectory measured by the single-beacon localization algorithm is compared with the reference trajectory, which is shown as follows:

$$\text{RMSE} = \sqrt{\frac{1}{n}\sum_{i=1}^{n}(L^i_{measured} - L^i_{reference})^2} \tag{34}$$

where $L^i_{measured}$ and $L^i_{reference}$ present positioning locations of single-beacon localization and DGPS, respectively. n stands for sampling number. As both the ship and beacon work at a fixed depth, the error of z direction can be ignored, hence the distance RMSE can be further expressed as

$$\begin{aligned} \text{RMSE} &= \sqrt{\frac{1}{n}\sum_{i=1}^{n}(L^i_{measured} - L^i_{reference})^2} \\ &= \sqrt{\frac{1}{n}\sum_{i=1}^{n}[(x^i_{measured} - x^i_{reference})^2 + (y^i_{measured} - y^i_{reference})^2]} \\ &= \sqrt{\frac{1}{n}\sum_{i=1}^{n}(x^i_{error} + y^i_{error})^2} \end{aligned} \tag{35}$$

where x^i_{error} and y^i_{error} indicate positioning error in x direction and y direction in the ith sampling, respectively.

In this experiment, based on distance RMSE, positioning errors of the proposed ANFIS-EKF and other existing algorithms, including EFK and ANFIS, are calculated. The results are shown in Figure 10 and Table 4.

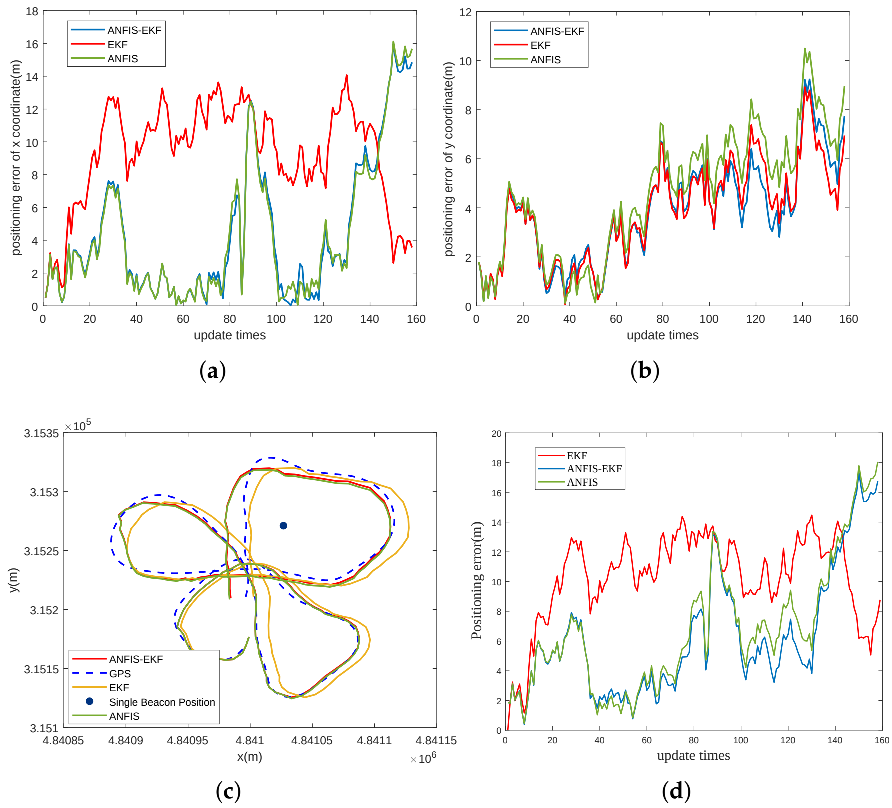

Figure 10. Performance analysis of ANFIS-EKF. (**a**) Positioning error comparison of x coordinate. (**b**) Positioning error comparison of y coordinate. (**c**) Estimated trajectories comparison. (**d**) Positioning error of DRMS.

Table 4. Positioning errors comparison of three methods.

Method	Error of x Direction (m)	Error of y Direction (m)	Error of DRMS (m)
EKF	9.2260	3.8170	10.3271
ANFIS	4.3264	4.5613	6.7529
ANFIS-EKF	4.3275	3.8053	6.1890

From Figure 10 and Table 4, it is clear that ANFIS-EKF performs the best in positioning accuracy among the three methods according to errors of DRMS. Furthermore, the improvement of positioning accuracy from EKF to ANFIS-EKF is different between the x direction and y direction, which is caused by ANFIS-EKF owning better ability to deal with values with large measuring errors. Moreover, compared with ANFIS, there is only relatively small improvement of ANFIS-EKF. However, it is known that the computation complexity of ANFIS is much bigger than EKF. Hence, the joint ANFIS-EKF can decrease computation complexity more greatly than only adopting ANFIS in single-beacon localization.

The influence of parameters shown in Table 1 are analyzed in the following. Input membership function type and training times are discussed, respectively.

Figure 11 gives the trajectory comparison of three commonly used membership function types in ANFIS, including Trimf, Gbellmf ,and Trapmf, which are described in detail in [29]. The statistical positioning errors of Trimf, Gbellmf, and Trapmf are 7.0102 m, 70.8683 m, and 71.5888 m, respectively. It is clear that Trimf performs best among the three types. It is well known that membership function type represents the characteristic of studied objects in fuzzy logic, and the relationship of velocity information and positioning result needs high-resolution and high control sensitivity of the membership function; moreover, Trimf is the most suitable for sharper curves, hence Trimf is the most optimal choice in ANFIS-EKF.

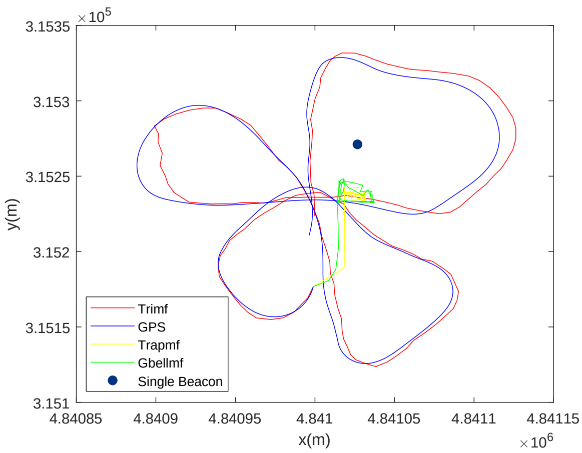

Figure 11. Comparsion of different membership function types

Then, an experiment is conducted to analyze the influence of training length. Training length presents the number of times for ANFIS to obtain the model of the current system. A further time period for the whole training process can be achieved by multiplying training length with cycle period. An appropriate training length cannot only obtain the best model but also saves calculating complexity. Three training lengths of 80, 120, and 150 were set, respectively, according to the actual length of field data. Figure 12 and Table 5 gives the experiment results.

On the whole, bigger training lengths bring higher positioning accuracies for ANFIS or ANFIS-EKF. When training lengths arrive at big enough values, ANFIS-EKF performs the best among the three methods. It is benefiting from ANFIS-EKF inheriting the advantages of both ANIFS and EKF; furthermore, when training is large enough, the training network model can be infinitely close to the real model. Comparing the results of the 80 length and 120 length, it can be seen that positioning accuracy improves greatly. However, comparing the results of the 120 length and 150 length, the trend of improving slows down, which means the training model converges gradually.

In real applications, both completeness of the training model and computation complexity of different training lengths should be considered together. In the case of a larger number of data samples, a bigger training length should be adopted. Inversely, when there is only a small amount of field data that can be used, training length can be relatively reduced.

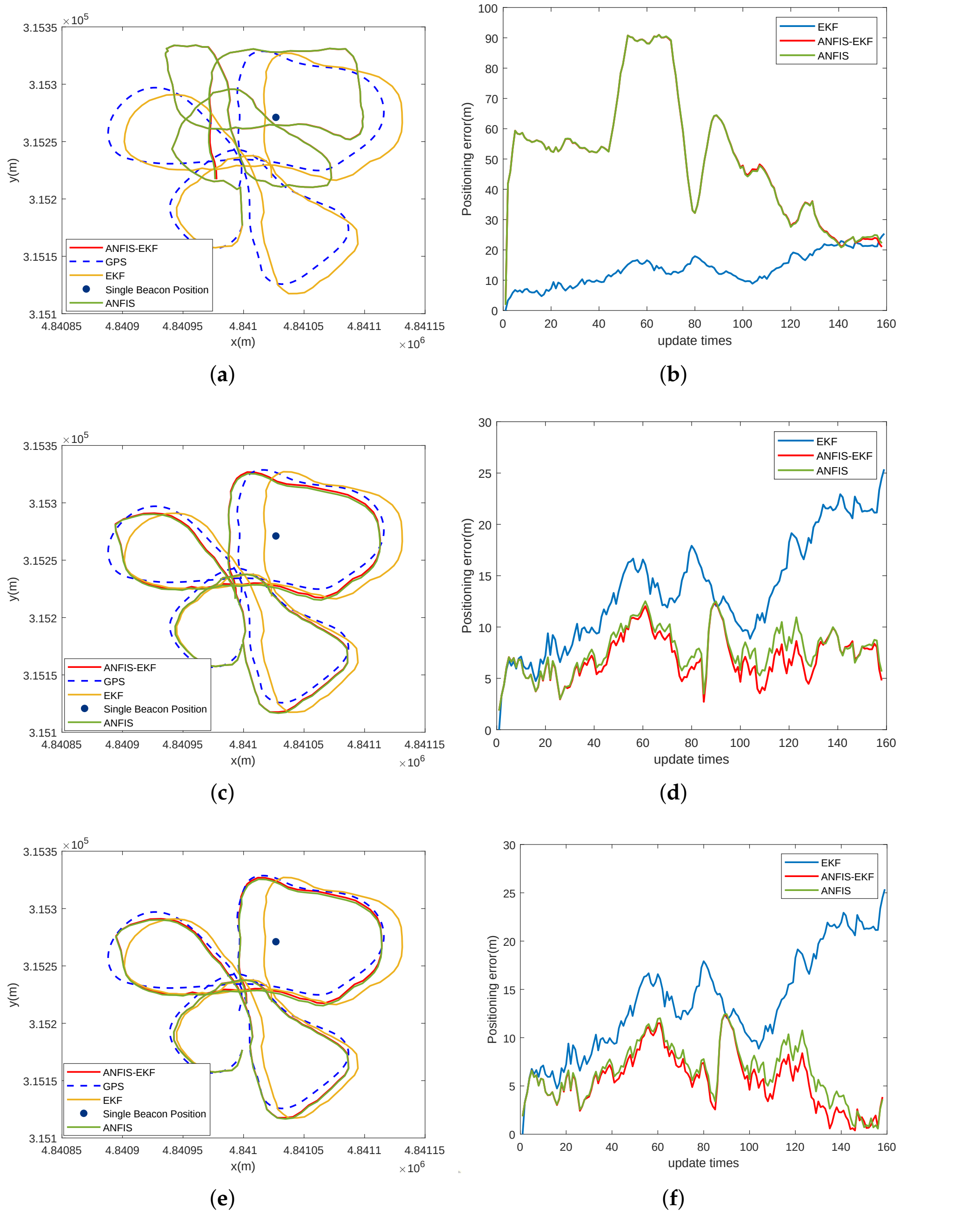

Figure 12. The experimental results of different training lengths. (**a**) Estimated trajectory of 80 training length. (**b**) Positioning error of 80 training length. (**c**) Estimated trajectory of 120 training length. (**d**) Positioning error of 120 training length. (**e**) Estimated trajectory of 150 training length. (**f**) Positioning error of 150 training length.

Table 5. The mean positioning error of different training lengths.

Method	Error of 80 Length (m)	Error of 120 Length (m)	Error of 150 Length (m)
EKF	13.6391	13.6391	13.6391
ANFIS	50.4973	7.7264	6.4113
ANFIS-EKF	50.1967	7.0206	5.6006

4. Conclusions

In this paper, a complete approach for single-beacon localization is investigated. A Multi-hypothesis Initial Position Discriminant (MHIPD) method is proposed to achieve accurate initial position, which gives significant support for initial observability. An improved EKF algorithm integrated with ANFIS is proposed to realize high-precision trajectory tracking in long-endurance operations of AUVs. Simulations and field experiments verify that the proposed MHIPD method is effective in initial observability measuring, and the proposed ANFIS-EKF method performs much better than traditional single-trajectory tracking algorithms.

In future works, more influence factors for underwater single-beacon localization will be studied, such as multi-path effects. Furthermore, we plan to refresh single-beacon localization technology itself, including using moving single beacons. More efficient schemes need to be studied further for various application scenarios.

Author Contributions: Conceptualization, W.Z.; data curation, H.Z.; formal analysis, G.Z.; project administration, G.L.; validation, H.Z.; investigation, W.Z.; writing—original draft, W.Z. All authors have read and agreed to the published version of the manuscript.

Funding: This work was supported in part by the National Natural Science Foundation of China (Grant No. 62101158), in part by the Shandong Provincial Natural Science Foundation (Grant No. ZR2021QF004), in part by the National Natural Science Foundation of China (Grant No. 61971156), in part by the Shandong Provincial Natural Science Foundation (Grant No. ZR2019MF035), and in part by the Shandong Provincial Natural Science Foundationan (Grant No. ZR2020MF141).

Data Availability Statement: Not applicable.

Conflicts of Interest: The authors declare no conflict of interest.

References

1. Xing, H.; Liu, Y.; Guo, S.; Shi, L.; Hou, X.; Liu, W.; Zhao, Y. A Multi-Sensor Fusion Self-Localization System of a Miniature Underwater Robot in Structured and GPS-Denied Environments. *IEEE Sens. J.* **2021**, *21*, 27136–27146. [CrossRef]
2. Scherbatyuk, A.P. The AUV positioning using ranges from one transponder LBL. In Proceedings of the OCEANS, '95 MTS/IEEE, San Diego, CA, USA, 9–12 October 1995; Volume 3, pp. 1620–1623.
3. Vaganay, J.; Baccou, P.; Jouvencel, B. Homing by acoustic ranging to a single-beacon. In Proceedings of the OCEANS 2000 MTS/IEEE Conference and Exhibition, Providence, RI, USA, 11–14 September 2000; Volume 2, pp. 1457–1462.
4. Vallicrosa, G.; Ridao, P. Sum of gaussian single-beacon range-only localization for AUV homing. *Annu. Rev. Control* **2016**, *42*, 177–187. [CrossRef]
5. De Palma, D.; Arrichiello, F.; Parlangeli, G.; Indiveri, G. Underwater localization using single-beacon measurements: Observability analysis for a double integrator system. *Ocean Eng.* **2017**, *142*, 650–665. [CrossRef]
6. Zhu, Z.B.; Hu, S.J. Model and algorithm improvement on single-beacon underwater tracking. *IEEE J. Ocean. Eng.* **2018**, *43*, 1143–1160. [CrossRef]
7. Deng, Z.C.; Yu, X.; Qin, H.D.; Zhu, Z.B. Adaptive Kalman filter-based single-beacon underwater tracking with unknown effective sound velocity. *Sensors* **2018**, *18*, 4339. [CrossRef]
8. Claus, B.; Kepper, J.H.; Suman, S.; Kinsey, J.C. Closed-loop one-way-travel-time navigation using low-grade odometry for autonomous underwater vehicles. *J. Field Robot.* **2018**, *35*, 421–434. [CrossRef]
9. Qin, H.D.; Yu, X.; Zhu, Z.B.; Deng, Z.C. An expectation-maximization based single-beacon underwater navigation method with unknown ESV. *Neurocomputing* **2019**, *378*, 295–303. [CrossRef]
10. Kepper, J.H.; Claus, B.C.; Kinsey, J.C. A navigation solution using a MEMS IMU, model-based dead-reckoning, and one-way-travel-time acoustic range measurements for autonomous underwater vehicles, *IEEE J. Ocean. Eng.* **2019**, *44*, 664–682. [CrossRef]
11. Sun, J.; Hu, F.; Jin, W.M.; Wang, J.; Wang, X.; Luo, Y.; Yu, J.; Zhang, A. Model-aided localization and navigation for underwater gliders using single-beacon travel-time differences. *Sensors* **2020**, *20*, 893. [CrossRef]
12. Yu, X.; Qin, H.D.; Zhu, Z.B. Globally exponentially stable single-beacon underwater navigation with unknown sound velocity estimation. *J. Frankl. Inst. Eng. Appl. Math.* **2021**, *358*, 2515–2534. [CrossRef]
13. Masmitja, I.; Gomariz, S.; Del-Rio, J.; Kieft, B.; O'Reilly, T.; Bouvet, P.J.; Aguzzi, J. Optimal path shape for range-only underwater target localization using a wave glider. *Int. J. Robot. Res.* **2018**, *37*, 1447–1462. [CrossRef]
14. Liu, H.M.; Wang, Z.J.; Zhao, S.; He, K. Accurate multiple ocean bottom seismometer positioning in shallow water using GNSS/Acoustic Technique. *Sensors* **2019**, *19*, 1406. [CrossRef] [PubMed]
15. Rahman, A.; Muthukkumarasamy, V. Embracing localization inaccuracy with a single-beacon. *Int. J. Adv. Comput. Sci. Appl.* **2019**, *10*, 452–459. [CrossRef]

16. Sun, S.B.; Zhang, X.Y.; Zheng, C.; Fu, J.; Zhao, C. Underwater acoustical localization of the black box utilizing single autonomous underwater vehicle based on the second-order time difference of arrival. *IEEE J. Ocean. Eng.* **2020**, *45*, 1268–1279. [CrossRef]
17. Sun, S.B.; Zhang, X.Y.; Zheng, C.; Zhao, C.; Fu, J. Underwater asynchronous navigation using single-beacon based on the phase difference. *Appl. Acoust.* **2021**, *172*, 107546. [CrossRef]
18. Larsen, M.B. Synthetic long baseline navigation of underwater vehicles. In Proceedings of the OCEANS 2000 MTS/IEEE Conference and Exhibition, Providence, RI, USA, 11–14 September 2000; Volume 3, pp. 2043–2050.
19. Lapointe C E. *Virtual Long Baseline (VLBL) Autonomous Underwater Vehicle Navigation Using a Single Transponder*; Massachusetts Institute of Technology: Cambridge, MA, USA, 2006.
20. Cao, J.; Han, Y.F.; Zhang, D.L.; Sun, D. Linearized iterative method for determining effects of vessel attitude error on single-beacon localization. *Appl. Acoust.* **2017**, *116*, 297–302. [CrossRef]
21. Masmitja, I.; Bouvet, P.J.; Gomariz, S.; Aguzzi, J.; del Rio, J. Underwater mobile target tracking with particle filter using an autonomous vehicle. In Proceedings of the OCEANS 2017, Aberdeen, UK, 19–22 June 2017; pp. 1–5.
22. Shaukat, N.; Ali, A.; Javed, I.M.; Moinuddin, M.; Orero, P. Multi-Sensor Fusion for Underwater Vehicle Localization by Augmentation of RBF Neural Network and Error-State Kalman Filter. *Sensors* **2021**, *21*, 1149. [CrossRef] [PubMed]
23. Ma, H.; Mu, X.; He, B. Adaptive Navigation Algorithm with Deep Learning for Autonomous Underwater Vehicle. *Sensors* **2021**, *21*, 6406. [CrossRef]
24. Or, B.; Klein, I. Adaptive Step Size Learning With Applications to Velocity Aided Inertial Navigation System. *IEEE Access* **2022**, *10*, 85818–85830. [CrossRef]
25. Jang, J.R. ANFIS: Adaptive-network-based fuzzy inference system. *IEEE Trans. Syst. Man Cybern.* **1993**, *23*, 665–685. [CrossRef]
26. Gharghan, S.K.; Nordin, R.; Ismail, M. A wireless sensor network with soft computing localization techniques for track cycling applications. *Sensors*, **2016**, *16*, 1043. [CrossRef] [PubMed]
27. Duan, Y.B.; Li, H.Z.; Wu, S.Q.; Zhang, K. INS error estimation based on an ANFIS and its application in complex and covert surroundings. *ISPRS Int. J. Geo-Inf.* **2021**, *10*, 388. [CrossRef]
28. Taek, L.S. Observability of target tracking with range-only measurements. *IEEE J. Ocean. Eng.* **1999**, *24*, 383–387. [CrossRef]
29. Kabir, M.; Kabir, M.M.J. Fuzzy membership function design: An adaptive neuro-fuzzy inference system (ANFIS) based approach. In Proceedings of the 2021 International Conference on Computer Communication and Informatics (ICCCI), Coimbatore, India, 27–29 January 2021; pp. 1–5.